Journal of Neuroscience Methods 138 (2004) 97–105

JOURNAL OF NEUROSCIENCE METHODS

www.elsevier.com/locate/jneumeth

Measuring fundamental frequencies in local field potentials

B. Masimore [a], J. Kakalios [a], A.D. Redish [b,*]

[a] *School of Physics and Astronomy, University of Minnesota, Minneapolis, MN 55455, USA*
[b] *Department of Neuroscience, University of Minnesota, 6-145 Jackson Hall, 321 Church Street SE, Minnneapolis, MN 55455, USA*

Received 28 August 2003; received in revised form 17 March 2004; accepted 17 March 2004

Abstract

Neural processes display rhythmic oscillations in local field potentials; identification of their characteristic frequencies is complicated due to their highly non-stationary nature. A simple technique, combining Fourier transforms and correlation coefficients yields unambiguous determinations of the frequencies without a priori filtering. This procedure also provides quantitative information concerning interactions between frequencies. Fundamental frequencies in local field potential data acquired from the hippocampus, cortex, and striatum from awake, behaving rats were calculated using this technique. Characteristic frequencies identified using this technique from hippocampus and cortex agreed with known oscillations. Application to dorsal striatal local field potentials identified a low-frequency theta component as well as a narrow gamma band oscillation at 50–55 Hz.

Keywords: Fundamental frequency; Oscillation; Gamma rhythm; Theta rhythm; $1/f$ Noise; Hippocampus; Postsubiculum; Striatum

1. Introduction

Oscillations have been proposed to underlie numerous fundamental computational components of information processing by neural systems (Buzsáki, 1989; Llinas, 2001; Llinas et al., 1999; Vanderwolf, 1971). Information carried by action potentials is enhanced by firing patterns which change in relation to the phase of an underlying rhythm (Carr et al., 1986; O'Keefe and Recce, 1993; Skaggs et al., 1996). These fundamental frequencies are indicative of underlying modes of the neural system (Klausberger et al., 2003; Llinas, 2001; Niedermeyer and Lopes da Silva, 1999; Vanderwolf, 1971). For example, changes in the hippocampal rhythm occur during awake, attentive states and slow-wave-sleep and non-attentive states (Buzsáki et al., 1983; O'Keefe and Nadel, 1978; Vanderwolf, 1971). The fundamental frequencies seen in extracranial EEG change during awake, sleep, and attentive states (Llinas, 2001; Niedermeyer and Lopes da Silva, 1999). Changes in the fundamental frequencies within a system can indicate disease states (Llinas, 2001; Llinas et al., 1999; Niedermeyer and Lopes da Silva, 1999). Parkinsonian states in basal ganglia structures produce oscillations at frequencies not seen in normal animals (Deuschl et al., 2000). Depression, schizophrenia, and other disease states produce abnormal oscillatory patterns in extracranial EEG (Llinas, 2001; Llinas et al., 1999; Niedermeyer and Lopes da Silva, 1999).

An important issue is thus the elucidation of the fundamental frequencies underlying rhythmic oscillations. Isolation of characteristic frequencies typically requires examination and filtering of large data files, involving assumptions of the frequency range in which one expects to observe these oscillations. This paper demonstrates that the correlation coefficients of the spectrogram of time-series data, which have previously been employed to characterize physical phenomena such as conductance fluctuations in spin glasses (Weissman, 1988, 1993) and in hydrogenated amorphous silicon (Khera and Kakalios, 1997; Parman et al., 1992), enable identification of the fundamental frequencies of any transient rhythmic oscillations without the a priori assumptions required by filtering. In addition, this technique automatically provides information on the interactions between oscillators, which is not readily available using filtering methods.

* Corresponding author. Tel.: +1-612-626-3738; fax: +1-612-626-5009.
E-mail address: redish@ahc.umn.edu (A.D. Redish).

0165-0270/$ – see front matter © 2004 Elsevier B.V. All rights reserved.
doi:10.1016/j.jneumeth.2004.03.014

2. Materials and methods

2.1. Overview of technique

Standard techniques for identifying fundamental frequencies typically entail applying a fast Fourier transform (FFT) to the time-series and then examining either the power spectrum or the spectrogram. The power spectrum assumes that the data are stationary in time, an assumption that is invalid for almost all neural data. Non-stationary oscillations are difficult to identify within an average power spectrum because the characteristic frequency peak only occurs in a limited number of time-windows. Averaging across time-windows dilutes the magnitude of the characteristic peak so that it may be difficult to resolve from background fluctuations. The spectrogram does not assume stationarity, in that it measures the power at each frequency as a function of time, but examining a spectrogram for a long data session is extremely difficult because each time-window contributes one column to the spectrogram. In addition, since neural data tend to have a low signal-to-noise ratio, identifying the fundamental frequencies within each time-window can be difficult.

Instead of averaging the separate samples of the spectrogram, we propose correlating the power values at each frequency across the time samples within the spectrogram. For Gaussian processes, the two-point autocorrelation function contains all the relevant information concerning the physical processes underlying the fluctuating time-series (Dutta and Horn, 1981; Kogan, 1996), as the magnitude of the FFT amplitudes at one frequency are uncorrelated with the FFT amplitudes at another frequency (Khera and Kakalios, 1997). However, interactions between fluctuators can produce significant time-dependent variations in the power spectra with non-trivial correlations. These can be quantified through the calculation of a conventional correlation coefficient ρ_{ij}, where the indices i and j denote differing frequencies within the same time-series. Since any characteristic oscillation arising from a biological rhythm will have a finite, non-zero width, it will overlap with adjacent frequencies, and thus will show a non-zero correlation with neighboring frequencies, even if it does not interact with other oscillations.

2.2. Detailed methods

Local field potentials (LFPs) were recorded from tetrodes chronically implanted in awake, behaving rats as the animals performed spatial tasks. Tetrodes were implanted in the hippocampus (two rats), the postsubiculum (cortex; two rats), or the dorsal striatum (five rats). Local field potentials were recorded with 16 channels of a Cheetah 54-channel system (Neuralynx, Tucson, AZ). Signals were amplified at unity-gain at a head-stage (Neuralynx) directly connected to the implant. Signals passed through shielded cables and a 72-channel commutator to a pair of Lynx-8 amplifiers (500×, Neuralynx), processed through the Cheetah A2D processor, and stored at a sampling frequency of 943 or 2003 Hz. All local field potential signals were filtered at 1–475 Hz in the amplifiers.

Tetrodes were made from 14 μm NiChrome wire (Kanthal Precision Wire, Palm Coast, FL). Tetrodes were loaded into hyperdrives (David Kopf Instruments, Tujunga, CA), providing individual microdrives for each of 12 tetrodes and 2 single-wire electrodes used as references for common noise rejection. Hyperdrives were implanted stereotactically over the target location (hippocampus: Bregma −3.8 mm AP, +2.0 mm ML; postsubiculum: Bregma −7.0 mm AP, +2.4 mm ML; dorsal striatum: Bregma +0.5 mm AP, 3.0 mm ML). Surgery was done under general anesthesia (sodium pentobarbital 40–50 mg/kg, maintained with isoflurane 0.5–2%, vaporized into pure oxygen, delivered at 1.0 L/min) and under sterile conditions. Signals were measured relative to a ground screw implanted during surgery in the parietal bone. After surgery, electrodes were lowered into place over the subsequent 1–3 weeks.

2.2.1. Analysis methods

The time-dependent fluctuations of the voltages $V(t)$ recorded from the tetrodes were first broken into individual, continuous, contiguous, non-overlapping time-windows. The extent of the time-window determined the lowest frequency in the Fourier transform of $V(t)$, while the data acquisition rate constrained the upper frequency. The voltage was fast Fourier transformed and then multiplied by its complex conjugate, to yield the spectral density as a function of frequency. This was done for a number of successive time-windows; typically 256 time-windows were used.

The correlation between the power spectrum $S(f)$ at a frequency f_i and at another frequency f_j can be calculated using the expression

$$\rho_{ij} = \frac{\sum_k (S_k(f_i) - \langle S(f_i)\rangle)(S_k(f_j) - \langle S(f_j)\rangle)}{\sigma_i \sigma_j} \quad (1)$$

where $S_k(f_i)$ is the spectral density at frequency f_i in time-window k, $\langle S(f_i)\rangle$ the average spectral density magnitude at frequency f_i over all time-windows, σ_i the standard deviation of the spectral density at frequency f_i, and k ranges over the 256 time-windows. Because the spectral density at any frequency will always be perfectly correlated with itself, ρ_{ii} will always be unity. Time-windows in which the recorded voltage exceeded the maximum range of the analog-to-digital converter were omitted from the correlation coefficient calculation.

These correlations can be visualized through standard correlation plots (Figs. 1C and F and 2–4). Correlation coefficient values of zero are shown in white, while high correlations are shown dark. No significant anti-correlations ($\rho_{ij} < 0$) were found. In these plots, the diagonal represents ρ_{ii} and thus has a value of 1 by definition. Since $\rho_{ij} = \rho_{ji}$, the upper triangle of these plots are redundant with the corresponding lower triangles, but have been included for convenience. Biologically-generated fundamental frequencies appear as areas of high correlation and are reflected by symmetric gray

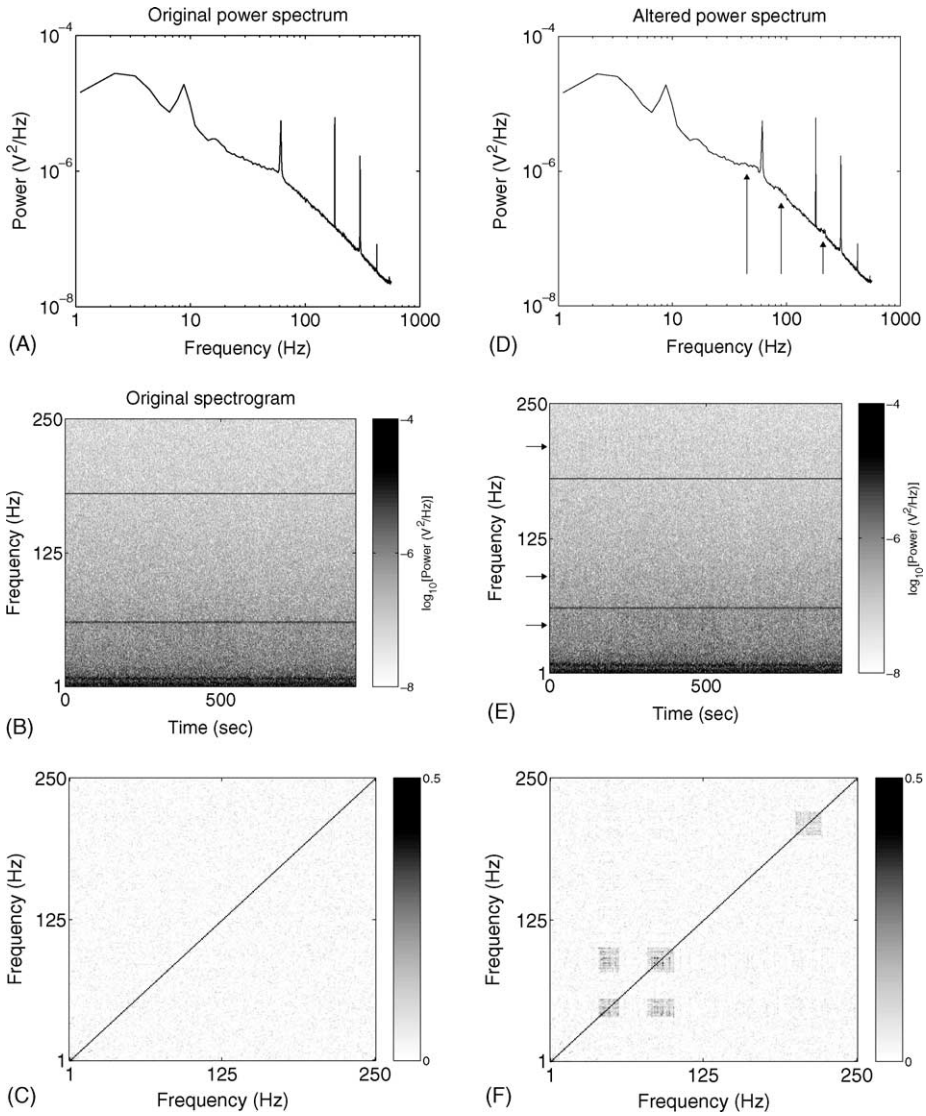

Fig. 1. Simulation. Voltage values from a single electrode channel showing Gaussian $1/f$ noise characteristics were recorded forming a base time-series (A–C). As can be clearly seen in the power spectrum (A) and the spectrogram (B), the sample showed strong 60 Hz oscillations with the corresponding harmonics. The correlation plot shows that the channel consisted of Gaussian fluctuators with no fundamental frequencies (C). This is typical of electrical noise sources (Dutta and Horn, 1981; Kogan, 1996). Two independent, intermittent fluctuators were added to the time-series, one with components at 40–55 and 80–100 Hz, the other with a component at 200–220 Hz (D–F). These fluctuators can be seen as small peaks in the power spectrum (D), but they are swamped by the 60 Hz noise. Because they were added intermittently, they are nearly invisible in the spectrogram (E). However, the correlation plot (F) clearly shows three fundamental frequencies, two of which were related to each other. Arrows indicate the inserted frequencies in the power spectrum (D) and the spectrogram (E). The diagonal in panel (C) represents ρ_{ii} and thus has a value of 1 by definition. The Gaussian nature of the $1/f$ noise is reflected in the fact that $\rho_{ij} = 0$ for all $i \neq j$ in panel (C). Since $\rho_{ij} = \rho_{ji}$, the upper triangle of panels (C) and (F) are redundant with the corresponding lower triangles, however, they have been included for convenience. The areas of high correlation are reflected by the gray squares in panel (F) and correspond to the frequencies indicated by the arrows in panel (D).

squares near the diagonal. Off-axis dark regions indicate interactions between oscillators. Non-biological noise appears as sharp, uncorrelated lines in these plots.

2.2.2. Experimental methods

All animals used were Brown Norway Hybrid rats (age 7–18 months at time of recording). Animals were handled 15 min daily. All procedures were approved by the IACUC at the University of Minnesota and were in accordance with NIH guidelines for animal care.

The data in this study came from rats trained on a number of different behavioral tasks. The hippocampal data was taken from rats performing Linear Track (O'Keefe and Recce, 1993), Open Field (Muller et al., 1987), and Open Field Goal (Olypher et al., 2002) tasks. The postsubicular data came from rats performing the Open Field (Muller et al., 1987; Taube et al., 1990) task. The dorsal striatal data came from rats performing Multiple-T (Schmitzer-Torbert and Redish, 2002) and NosePoke (Jackson et al., 2002) tasks. In the Linear Track task, rats ran back and forth on

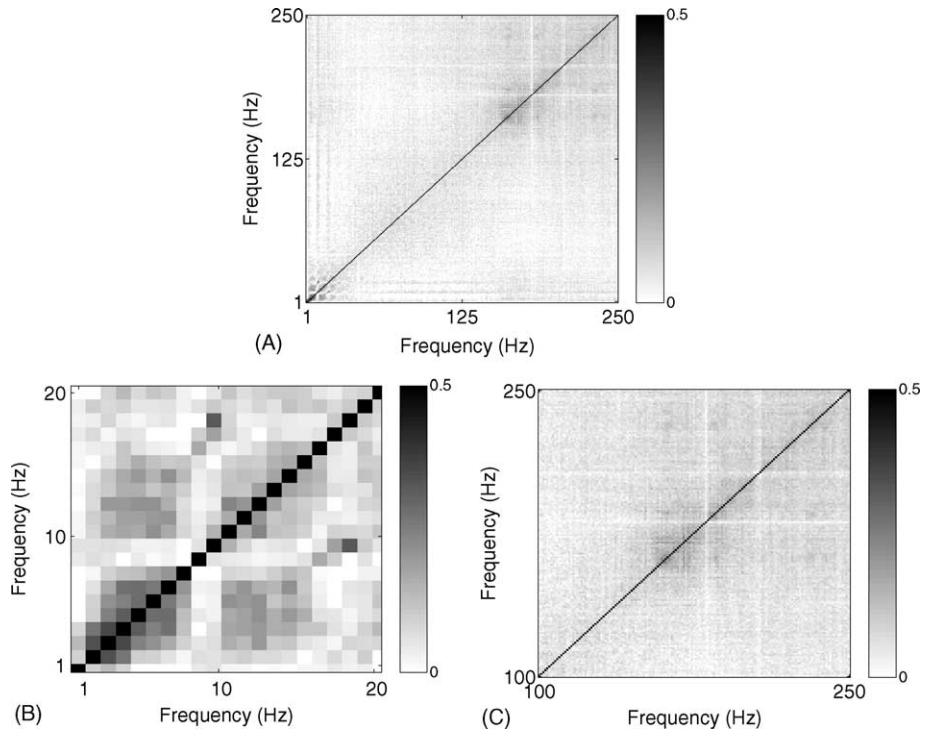

Fig. 2. Correlation structure of local field potentials recorded from the hippocampal pyramidal layer of two rats. (A) Correlation matrix of all frequencies ranging from 1 to 250 Hz. Note the clear blocks in the low-frequency (0–20 Hz) and high-frequency (160–220 Hz) ranges. (B) Expanded plot of the correlation matrix of the frequencies ranging from 1 to 20 Hz. Note the strong 5–15 Hz oscillator (theta). The uncorrelated 10 Hz oscillator (with its 20 Hz harmonic) is non-biological; it is generated by the firing of automated pellet-delivery feeders during the behavioral task. (C) Expanded plot of the correlation matrix ranging from 100 to 250 Hz. Note the 160–220 Hz component.

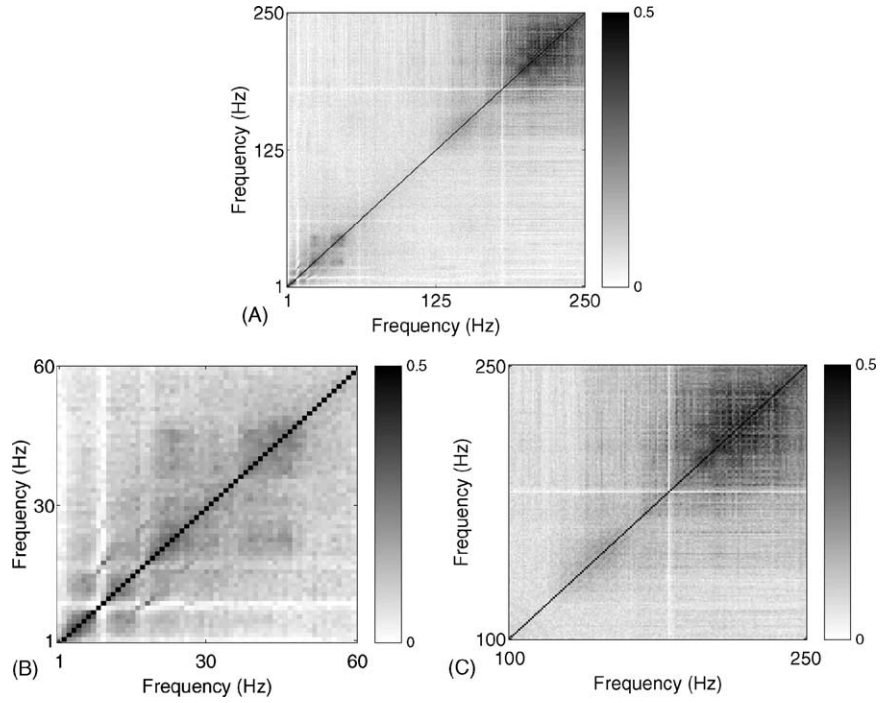

Fig. 3. Correlation structure of local field potentials recorded from the postsubiculum of two rats. (A) Correlation matrix of all frequencies ranging from 1 to 250 Hz. Note the regions in the low-frequency range (1–60 Hz) and in the high-frequency range (120–160 Hz), as well as the strong >200 Hz components. (B) Expanded correlation matrix showing the substructure in the low-frequency range. The uncorrelated signal occurring at 10 Hz is non-neural noise generated by the automated pellet-delivery system. (C) Expanded correlation matrix showing the 120–160 Hz component and the >200 Hz component. The uncorrelated signal occurring at 180 Hz is an odd harmonic of the 60 Hz non-neural noise.

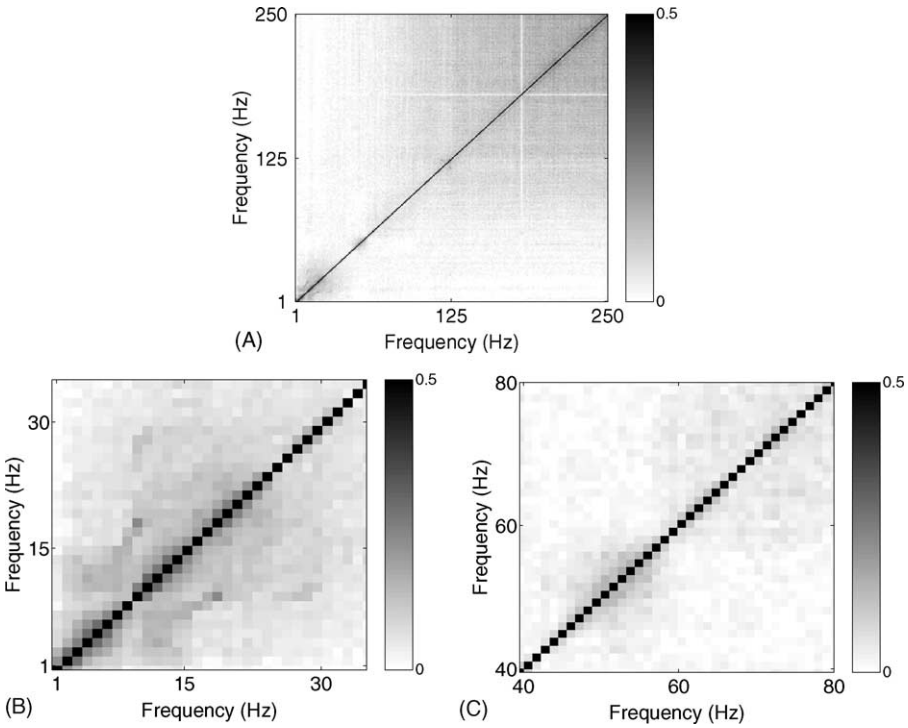

Fig. 4. Correlation structure of local field potentials recorded from the dorsocentral striatum. (A) Correlation matrix of all frequencies ranging from 1 to 250 Hz. Note the clear blocks in the low-frequency range (1–30 Hz), in the gamma band range (50–55 Hz). (B) Expanded plot showing the substructure in the low-frequency range. (C) Expanded plot showing the tight fluctuator in the mid-frequency range.

a 1.25 m linear track, receiving food at both ends. In the Open Field task, animals foraged for food in a 1 m diameter cylinder with a cue-card subtending 90°. Food was delivered randomly with a Poisson interval ($\lambda = 10$ s). In the Open Field Goal task, rats also foraged for food in the 1 m cylinder, but food was only delivered when rats crossed a 7 cm diameter goal region. The goal was re-armed only after rats had been outside of a 14 cm diameter region around the goal for 4 s. In the Multiple-T task, rats ran through a sequence of four T-choices in order to receive food. The last choice led to a return path, so the task entailed running a 4 m loop for food. In the NosePoke task, a rat had to hold his nose in a nose-poke port in order to break an LED beam. If the LED beam was interrupted for 500 ms, food became available at the other end of the 1.25 m track. The beam was not re-armed until the rat had traveled to the other end of the track and received its food. Sessions ran from 20 to 40 min, depending on specifics of the task. These data thus come from a variety of behavioral tasks, including spatial, navigational, and operant-conditioning tasks.

3. Results

This simple methodology provides a novel means of determining the fundamental oscillation frequencies within a neural structure. In Sections 3.1–3.4, we first test this method with simulations, inserting known fluctuators into an example recording. We then show that in hippocampus, in which the characteristic LFP oscillation frequencies are well-known, this method identifies the known frequencies. We then apply the method to a new aspect of a structure with known oscillations (postsubiculum, part of cortex). Postsubiculum showed oscillation components similar to other aspects of cortex. Finally, we apply the method to the dorsal striatum, where the fundamental LFP oscillation frequencies are unknown, and identify novel oscillatory components there.

3.1. Simulation

In order to test the capabilities of the method proposed here, simulations were used to create a time-series in which all frequencies present were known. Applying the method to these simulations indicated that fundamental oscillations can be detected in correlation coefficients even while remaining invisible using standard frequency analysis techniques.

A single voltage time-series from a single tetrode channel was recorded from an animal performing the NosePoke task. One thousand and twenty-four traces of 1024 sequential data points were analyzed. Only the data for which the animal was on task were included and any traces for which the signal exceeded the recording threshold were rejected. The first 1024 traces that met both of these criteria were then used. Each trace was then Fourier transformed and the power spectrum calculated as discussed previously. The

resulting power spectra were then averaged and analyzed sequentially as a spectrogram. Correlations coefficients were then calculated using Eq. (1) and it was observed that this sample exhibited uncorrelated, Gaussian noise.

The single voltage time-series from the single tetrode channel that was analyzed exhibited completely Gaussian $1/f$ noise (Fig. 1). (A spectral density is considered *Gaussian* if it arises from a large number of statistically independent fluctuators, so that the magnitude of the spectral density at one frequency is uncorrelated with the power spectrum at a differing frequency.) In the first spectra, external electrical noise was observed as sharp peaks at 60 Hz and the odd harmonics. Three components were then added to 100 randomly selected time-windows out of the 1024 windows included in the time-series. Two of the components (40–55 and 80–100 Hz) were added during the same randomly selected times while the third component (200–220 Hz) was placed in a different set of randomly selected time-window traces.

As shown in Fig. 1D, the fluctuators were evident in the first spectra, but were not dominant features, especially when compared to the presence of other prominent features such as strong electrical noise. The spectrogram (Fig. 1E) yielded no new information. However, the correlation matrix (Fig. 1F) unambiguously showed fluctuators at the appropriate three frequencies. The off-axis region of correlation (between 40–55 and 80–100 Hz) indicates that those two fluctuators showed high power at similar times, implying that the two fluctuators were likely to have been coupled and may have arisen from a single process. The absence of off-axis correlations between the third fluctuator (200–220 Hz) and either of the others indicates that they were uncoupled and unlikely to have arisen from the same process. The figures shown were generated by placing fluctuators in less than 10% of the traces and amplifying the noise power by a factor of two—a conservative estimate compared to the amplitude of fundamental oscillations in local field potentials taken from neural structures such as hippocampus.

3.2. Hippocampus

Local field potentials recorded from the stratum pyramidale of the hippocampus show two major oscillatory frequencies, theta (7–14 Hz), occurring during awake, attentive and REM states (O'Keefe and Nadel, 1978; Vanderwolf, 1971), and ripples (200 Hz) (Ylinen et al., 1995), which ride on sharp-waves that occur during slow-wave-sleep and inattentive states (Buzsáki et al., 1983). Other oscillations can also be seen in hippocampal structures (such as gamma oscillations; 50–100 Hz) (Bragin et al., 1995), but these do not show strong power in stratum pyramidale (Csicsvari et al., 2003). In order to test the capabilities of our proposed method to identify fluctuators in real situations, we measured local field potentials from tetrodes chronically implanted in the dorsal hippocampal pyramidal layer.

As can be seen in Fig. 2, there were clear regions of high activity in the low-frequency range (0–20 Hz) and in a high-frequency range (160–220 Hz). Examination of the low-frequency range showed a strong fluctuator at 5–15 Hz, likely to have been the theta signal. The very sharp, uncorrelated 10 Hz signal slicing through this is non-biological; it was generated by the firing of automated pellet-delivery feeders. The high-frequency power block is likely to have arisen from ripples which typically show oscillations in the range of 140–200 Hz (Chrobak et al., 2000; Ylinen et al., 1995).

The local field potential oscillation structure of hippocampus is well known, and our method found the key frequencies therein. We next apply the method to a structure where the specific frequencies are not known, but can be inferred from similar structures.

3.3. Postsubiculum (cortex)

Fundamental oscillatory frequencies have been well-studied in cortex, particularly through extracranial EEG (Niedermeyer and Lopes da Silva, 1999) and in local field potentials recorded in primary visual cortex (Gray and Singer, 1989; Singer and Gray, 1995). The strongest oscillatory component of cortex is the well-studied 40 Hz gamma band (Gray and Singer, 1989; Niedermeyer and Lopes da Silva, 1999; Pesaran et al., 2002; Schanze and Eckhorn, 1997; Sewards and Sewards, 1999). Other slower components have also been identified, including theta (4–8 Hz) (Kahana et al., 2001; Niedermeyer and Lopes da Silva, 1999; Sewards and Sewards, 1999), alpha (8–13 Hz) (Niedermeyer and Lopes da Silva, 1999; Schanze and Eckhorn, 1997; Sewards and Sewards, 1999), and beta (14–30 Hz) (Niedermeyer and Lopes da Silva, 1999; Schanze and Eckhorn, 1997; Sewards and Sewards, 1999). Although other aspects of cortex have been extensively studied, we know of no studies of the local field potentials in postsubiculum. The data presented below suggest that postsubiculum shows local field potential oscillations similar to other aspects of cortex.

As can be seen in Fig. 3, there were three regions of non-zero correlations, a region showing complex substructure in the low ranges (1–60 Hz), a 130–160 Hz region, as well as high-frequency components (>200 Hz). The low-frequency region contained a complex substructure, including a smaller 5–10 Hz region (theta), and an anti-correlated 10 Hz component (non-biological, arising from automated pellet-delivery feeders). In addition the correlation matrix showed a strong 20–50 Hz (gamma) component. The identification of a 150 Hz fundamental oscillation is novel, but there have been reports of high-frequency oscillations >200 Hz in other aspects of rodent cortex (Barth, 2003; Grenier et al., 2001; Jones and Barth, 1999). There have been no previous studies of local field potentials in postsubiculum, but the results presented here suggest that postsubiculum shows oscillatory com-

ponents similar to other aspects of cortex, rather than to hippocampus.

3.4. Striatum

Fundamental oscillatory frequencies have not been well-studied in the dorsal striatum, however, preliminary reports of striatal rhythms have been reported. DeCoteau et al. (2002) have reported that a theta oscillation (7–10 Hz) can be seen under certain conditions and Berke et al. (2003) have reported the presence of gamma-band oscillations (35–100 Hz). We recorded local field potentials from five rats running a variety of behavioral tasks (see Section 2 for details).

The correlation matrix (Fig. 4) identified two clear regions of important frequencies (1–30 and 50–55 Hz). The lack of off-axis correlations between the two regions indicate that these fluctuators were likely to have been generated by different processes.

Although the correlation matrix does not tell us when the characteristic oscillations appear, nor under what conditions they occur, nor what the behavioral correlates of the frequencies are, it can guide our investigation to look at the fundamental frequencies identified here. The gamma band is traditionally specified as being very broad (30–100 Hz) (Bragin et al., 1995; Csicsvari et al., 2003; Friedman-Hill et al., 2000; Gothard et al., 2001; Rodriguez et al., 1999; Singer and Gray, 1995). The data reported here identify the important oscillatory range in striatum as extremely tight (50–55 Hz).

4. Discussion

This paper provides a novel methodology for determining the fundamental frequency of a neural time-series, such as the local field potential. By combining two well-understood techniques in common use in neuroscience (Fourier transforms and correlation coefficients), it provides an easily accessible procedure applicable to many aspects of neuroscience. The key advantage over other techniques for determining fundamental underlying frequencies is that it allows the averaging of multiple time-windows from long data recordings to filter out noise effects, without making any assumptions about the stationarity of the data. This advantage makes this technique particularly useful for neural data, which tend to be non-stationary and to have a low signal-to-noise ratio.

While the technique of employing correlation coefficients to investigate local field potentials is not new (Baccalá and Sameshima, 2001; Gardner, 1992; Kocsis et al., 1999; Mitra and Pesaran, 1999; Niedermeyer and Lopes da Silva, 1999), we make use of a frequently overlooked property of the self-coherence function. Since any peak in the spectral density corresponding to the characteristic frequency of a rhythmic oscillation will have a finite, non-zero width (due to its transient nature), it can be identified by the finite cross-correlations with neighboring frequencies. The non-stationary, small amplitude aspect of these oscillations would ordinarily be buried in the background noise in a traditional average spectral density. In contrast, correlation coefficients are calculated by summing the correlations over a large number of individual power spectra. This summation leads to a cancellation of uncorrelated positive and negative coefficients, while a true correlated signal is undiluted by the summation process and is thereby readily detected.

4.1. Importance for other recording technologies

Neural oscillations appear in many data acquisition paradigms, including EEG, fMRI, MEG, and ensemble neural recordings. The techniques proposed in this paper are applicable to any time-series and will be of general use for all of these neural data.

4.2. Detection of non-neural noise sources

Any experimental set-up will include spurious non-neural noise arising from external sources. Experimental techniques to control such noise sources (e.g. 60 Hz and its harmonics) are a large part of any experimental project. Because these non-neural sources will be uncoupled from real neural fluctuators, they will appear as sharp uncorrelated bands in the correlation plot (e.g. see Fig. 3C). Because non-biological signals tend to be very sharp, the harmonics often also appear in the correlation plots. Off-axis correlations between a signal and its harmonics may suggest that the signal is non-biological. (For example, the 100 ms pulses used in the automated pellet feeders produced a non-biological 10 Hz signal and its corresponding 20 Hz harmonic (see Fig. 3B).) Our methodology provides an additional useful tool to identify real neural signals from non-neural noise sources. These signals can be difficult to disambiguate in power spectra.

4.3. Relation to coherence

The expression employed to calculate the correlation coefficient here (Eq. (1)) is sometimes referred to as *coherence* in the signal engineering community (Gardner, 1992). The correlation equation used here is mathematically equivalent to $\rho_{xy} = S_{xy}/\sqrt{S_{xx}S_{yy}}$, used for cross-spectral analysis (Leopold et al., 2003; Llinas et al., 1999; Niedermeyer and Lopes da Silva, 1999). S_{xy} is the cross-spectrum obtained by Fourier transforming the product of a time-dependent quantity $x(t)$ and the complex conjugate of another time-varying quantity $y(t)$, while S_{xx} and S_{yy} are the traditional spectral densities of $x(t)$ and $y(t)$, respectively. Previous use of the coherence function in neuroscience applications has involved cross-correlations between two spatially distinct probes, so that ρ_{xy} provides spatial correlation information (Baccalá and Sameshima, 2001; Bragin et al., 1995; Gardner, 1992;

Kocsis et al., 1999; Miltner et al., 1999; Niedermeyer and Lopes da Silva, 1999; Singer and Gray, 1995). In the present work, we employ the correlation coefficient to analyze the LFP data from a single electrode taking measurements from a single site. In this way the analysis presented here involves the *self-coherence* of the LFP signal, while previous investigators have studied the *mutual-spatial-coherence* function.

4.4. Relation to bispectral analysis

Bispectral analysis is widely used in EEG experiments to obtain information about the relative phases of oscillators (Niedermeyer and Lopes da Silva, 1999; Sigl and Chamoun, 1994). The methodology proposed here measures correlated changes in the power spectrum obtained by multiplying the Fourier transform by its complex conjugate. In contrast, in bispectral analysis, the real and imaginary components are considered separately. The bispectrum is a statistical calculation that yields information which is a mixture of amplitude and phase components. The bicoherence measurement provides strictly phase information just as correlation coefficients provide only amplitude information. The two techniques can thus, depending on the physical system, offer complementary information.

4.5. The choice of spectral estimation techniques

The method presented in this paper includes two parts: a transformation into the frequency domain and a subsequent statistical analysis of the quantity in the frequency domain. Multi-taper spectral analysis has been proposed as an alternative technique to analyze time-series neurobiological data (Llinas et al., 1999; Mitra and Pesaran, 1999). The relative merits of various spectral estimation techniques can be compared with respect to their bias and variance properties. The standard power spectrum used here (also known as the periodogram) is known to have poor bias due to broad power leakage through the spectrum. One way to improve the bias is to multiply the frequency term by a *taper* chosen to have desirable bias characteristics. While a taper could be almost any well behaved function, the Slepian sequences are often chosen for their independence characteristics (Mitra and Pesaran, 1999; Percival and Walden, 1993; Thomas, 1982). While a carefully chosen taper function can improve the bias, all tapers cause variance inflation. Multi-taper analysis utilizes the orthogonality of the Slepian sequences to effectively increase the sample set and thus decrease the variance, all while saving the bias improvements of the tapering (Percival and Walden, 1993; Thomas, 1982). Although this improves the bias, the variance still remains greater than that of the standard transform. In calculating correlations, the bias term is normalized out. Thus, improving the bias term does not improve correlations. In contrast, correlations are highly dependent on variance, and thus any inflation of the variance is problematic. For data looking only at first-order measures (such as power spectra), a multi-taper analysis may be a better choice (Mitra and Pesaran, 1999; Pesaran et al., 2002), but using multi-taper analysis does not improve correlation-based measures such as those described here.

5. Conclusion

In this paper, we describe generally-applicable techniques for identifying fundamental fluctuation frequencies in neural time-series data, without any a priori filtering assumptions. The proposed technique combines two well-understood neural analysis methods (Fourier transforms and correlation matrices), which will make the technique accessible to any neuroscientist. This technique is applicable to many neural data acquisition paradigms and should provide a useful tool for the analysis of neural data.

Acknowledgements

We thank Jadin Jackson, Neil Schmitzer-Torbert, Chris Boldt, Adam Johnson, and Kelsey Seeland for data collection. We thank T.J. Belich for assistance with the noise analysis. This research was supported by the University of Minnesota, by a University of Minnesota Graduate School grant for Interdisciplinary Research, Scholarly and Creative Activities, and by NIH (MH68029-01). Data collected for this analysis was partially funded by NSF-IGERT training grant #9870633 and by NIH (MH68029-01).

References

Baccalá LA, Sameshima K. Partial directed coherence: a new concept in neural structure determination. Biol Cybern 2001;84:463–74.

Barth DS. Submillisecond synchronization of fast electrical oscillations in neocortex. J Neurosci 2003;23(6):2502–10.

Berke J, Okatan, Skuski, Eichenbaum H. Synchronous striatal spindle and gamma oscillations in freely-moving rats. Soc Neurosci Abstr 2003 [program no. 390.16].

Bragin A, Jando G, Nadasdy Z, Hetke J, Wise K, Buzsáki G. Gamma (40–100 Hz) oscillation in the hippocampus of the behaving rat. J Neurosci 1995;15 (1):47–60.

Buzsáki G. Two-stage model of memory trace formation: a role for "noisy" brain states. Neuroscience 1989;31(3):551–70.

Buzsáki G, Leung LW, Vanderwolf CH. Cellular bases of hippocampal EEG in the behaving rat. Brain Res 1983;287(2):139-71.

Carr CE, Heiligenberg W, Rose GJ. A time-comparison circuit in the electric fish midbrain. I. Behavior and physiology. J Neurosci 1986;6(1):107–19.

Chrobak JJ, Lörincz A, Buzsáki G. Physiological patterns in the hippocampo-entorhinal cortex system. Hippocampus 2000;10:457–65.

Csicsvari J, Jamieson B, Wise KD, Buzsáki G. Mechanisms of gamma oscillations in the hippocampus of the behaving rat. Neuron 2003;37(311).

DeCoteau W, Courtemanche R, Kubota Y, Graybiel A. Anti-phase theta-range oscillations in striatum and hippocampus recorded in rats during T-maze task performance. Soc Neurosci Abstr 2002 [program no. 765.6].

Deuschl G, Raethjen J, Baron R, Lindemann M, Wilms H, Krack P. The pathophysiology of Parkinsonian tremor: a review. J Neurol 2000;247(Suppl 5):V/33–48.

Dutta P, Horn PM. Low frequency fluctuations in solids: $1/f$ noise. Rev Mod Phys 1981;53:497ff .

Friedman-Hill S, Maldonado PE, Gray CM. Dynamics of striate cortical activity in the alert macaque. I. Incidence and stimulus-dependence of gamma-band neuronal oscillations. Cereb Cortex 2000;10(11):1105–16.

Gardner WA. A unifying view of coherence in signal processing. Signal Process 1992;29:113–40.

Gothard KM, Hoffman KL, Battaglia FP, McNaughton BL. Dentate gyrus and CA1 ensemble activity during spatial reference frame shifts in the presence and absence of visual input. J Neurosci 2001;21(18):7284–92.

Gray CM, Singer W. Stimulus-specific neuronal oscillations in orientation columns of cat visual cortex. Proc Natl Acad Sci USA 1989;86(5):1698–702.

Grenier F, Timofeev I, Steriade M. Focal synchronization of ripples (80–200 Hz) in neocortex and their neuronal correlates. J Neurophysiol 2001;86(4):1884–98.

Jackson JC, Schmitzer-Torbert NC, Redish AD. Behavioral correlates of neuronal ensembles in dorsal striatum on a conditioned response task. Soc Neurosci Abstr 2002 [program no. 676.5].

Jones MS, Barth DS. Spatiotemporal organization of fast (>200 Hz) electrical oscillations in rat vibrissa/barrel cortex. J Neurophysiol 1999;82(3):1599–609.

Kahana MJ, Seelig D, Madsen JR. Theta returns. Curr Opin Neurobiol 2001;11(6):739–44.

Khera GM, Kakalios J. Temperature and doping dependence of non-Gaussian $1/f$ noise and noise statistics in hydrogenated amorphous silicon. Phys Rev B 1997;56:1918–27.

Klausberger T, Magill PJ, Márton LF, Roberts JDB, Cobden PM, Buzsáki G, Somogyi P. Brain-state and cell-type-specific firing of hippocampal interneurons in vivo. Nature 2003;421:844–8.

Kocsis B, Bragin A, Buzsaki G. Interdependence of multiple theta generators in the hippocampus: a partial coherence analysis. J Neurosci 1999;19(14):6200–12.

Kogan S. Electronic noise and fluctuations in solids. Cambridge, UK: Cambridge University Press; 1996.

Leopold DA, Murayama Y, Logothetis NK. Very slow activity fluctuations in monkey visual cortex: Implications for functional brain imaging. Cereb Cortex 2003;13:422–33.

Llinas RR. I of the vortex. MIT Press; 2001.

Llinas RR, Ribary U, Jeanmonod D, Kronberg E, Mitra PP. Thalamocortical dysrhythmia: a neurological and neuropsychiatric syndrome characterized by magnetoencephalography. Proc Natl Acad Sci USA 1999;96(26):15222–7.

Miltner WHR, Braun C, Arnold M, Witte H, Taub E. Coherence of gamma-band EEG activity as a basis for associative learning. Nature 1999;397:434–6.

Mitra PP, Pesaran B. Analysis of dynamic brain imaging data. Biophys J 1999;76:691–708.

Muller RU, Kubie JL, Ranck Jr JB. Spatial firing patterns of hippocampal complex-spike cells in a fixed environment. J Neurosci 1987;7:1935–50.

Niedermeyer E, Lopes da Silva F, editors. Electroencephalography: basic principles, clinical applications, and related fields. 4th ed. Baltimore, MD: Williams & Wilkins; 1999.

O'Keefe J, Nadel L. The hippocampus as a cognitive map. Oxford: Clarendon Press; 1978.

O'Keefe J, Recce M. Phase relationship between hippocampal place units and the EEG theta rhythm. Hippocampus 1993;3:317–30.

Olypher AV, Lánský P, Fenton AA. Properties of the extra-positional signal in hippocampal place cell discharge derived from the overdispersion in location-specific firing. Neuroscience 2002;111(3):553–66.

Parman CE, Israeloff NE, Kakalios J. Conductance noise power fluctuations in hydrogenated amorphous silicon. Phys Rev Lett 1992;69(7):1097–100.

Percival DB, Walden AT. Spectral analysis for physical applications: multitaper and conventional univariate techniques. Cambridge, UK: Cambridge University Press; 1993.

Pesaran B, Pezaris JS, Sahani M, Mitra PP, Andersen RA. Temporal structure in neuronal activity during working memory in macaque parietal cortex. Nat Neurosci 2002;5:805–11.

Rodriguez E, George N, Lachaux JP, Martinerie J, Renault B, Varela FJ. Perception's shadow: long-distance synchronization of human brain activity. Nature 1999;397:430–3.

Schanze T, Eckhorn R. Phase correlation of cortical rhythms at different frequencies: higher-order spectral analysis of multiple-microelectrode recordings from cat and monkey visual cortex. Int J Psychophysiol 1997;26(1–3):171–89.

Schmitzer-Torbert NC, Redish AD. Development of path stereotypy in a single day in rats on a multiple-T maze. Arch Ital Biol 2002;140:295–301.

Sewards TV, Sewards MA. Alpha-band oscillations in visual cortex: part of the neural correlate of visual awareness? Int J Psychophysiol 1999;32(1):35–45.

Sigl JC, Chamoun NS. An introduction to bispectral analysis for the electroencephalogram. J Clin Monit 1994;10:392–404.

Singer W, Gray CM. Visual feature integration and the temporal correlation hypothesis. Annu Rev Neurosci 1995;18:555–86.

Skaggs WE, McNaughton BL, Wilson MA, Barnes CA. Theta phase precession in hippocampal neuronal populations and the compression of temporal sequences. Hippocampus 1996;6(2):149–73.

Taube JS, Muller RU, Ranck Jr JB. Head direction cells recorded from the postsubiculum in freely moving rats. I. Description and quantitative analysis. J Neurosci 1990;10:420–35.

Thomas DJ. Spectrum estimation and harmonic analysis. Proc IEEE 1982;70:1055–96.

Vanderwolf CH. Limbic-diencephalic mechanisms of voluntary movement. Psychol Rev 1971;78(2):83–113.

Weissman MB. $1/f$ Noise and other, slow nonexponential kinetics in condensed matter. Rev Mod Phys 1988;60:537–71.

Weissman MB. What is a spin glass? A glimpse via mesoscopic noise. Rev Mod Phys 1993;65:829–39.

Ylinen A, Bragin A, Nadasdy Z, Jando G, Szabo I, Sik A, Buzsáki G. Sharp wave-associated high-frequency oscillation (200 Hz) in the intact hippocampus: Network and intracellular mechanisms. J Neurosci 1995;15(1):30–46.